

REAL-TIME GEOMETRY ASSESSMENT USING LASER LINE SCANNER DURING LASER POWDER DIRECTED ENERGY DEPOSITION ADDITIVE MANUFACTURING OF SS316L COMPONENT WITH SHARP FEATURE

Liu Yang, Boyu Wang & Jack C. P. Cheng

Department of Civil and Environmental Engineering, The Hong Kong University of Science and Technology, Clear Water Bay, Kowloon, Hong Kong

Peipei Liu

School of Civil Engineering, Southeast University, Nanjing, 210096, China

Hoon Sohn

Department of Civil and Environmental Engineering, Korea Advanced Institute of Science and Technology (KAIST), Daejeon, 34141, Republic of Korea

ABSTRACT: Directed energy deposition (DED) is a major metal additive manufacturing (AM) technology that is increasingly used in many industries due to its ability to manufacture complex components of arbitrary shapes and sizes. However, a lack of timely geometry assessment and the consequent geometry control hinders the development of DED towards zero defect manufacturing. In this study, a real-time geometry assessment methodology is developed for laser powder directed energy deposition (LP-DED). A geometry assessment system is developed using a laser line scanner capable of inspecting the melt pool area, the just solidified area, as well as layer-wise inspection. An image processing method with an encoder-decoder based profile completion network was developed to obtain accurate track profile in images from real-time inspection. Experiments have been conducted to validate the proposed methodology by depositing multi-layer X-shape objects.

KEYWORDS: Additive Manufacturing, Directed energy deposition, Real-time geometry assessment, Laser line scanning

1. INTRODUCTION

Metal additive manufacturing (AM) technologies' potential to revolutionize the manufacturing industry has not only been well-recognized but has inspired many fields [1]. According to the American Society for Testing and Materials (ASTM) standard [2], the two main groups of metal additive manufacturing technologies are directed energy deposition (DED) and powder bed fusion (PBF), both of which have been widely applied in, for example, the aerospace, automobile, and biomedical industries. In recent years, DED has gained attention as a viable manufacturing method in the construction industry where metallic materials are used extensively in distinctive and complex designs [3]. Often, traditional techniques such as hot rolling, cold forming, and extrusion can only produce regularly shaped, prismatic metallic components [4], which limits the potential use of metallic materials in construction and design. DED can complement traditional methods and produce components with almost any shapes with high precision.

However, DED is somewhat plagued by geometry problems [5]. For example, the thicknesses of the deposited ("printed") layers often deviate from their design values [6]. When more and more layers are deposited, heat accumulation tends to cause the layers to spread, increasing their width but decreasing their height [7]. In addition, as the nozzle comes to deposit the object's corners or intersections, the resulting geometry also quite often deviates from the design [8]. The geometrical dimensions of the deposited object often fail to meet the quality requirement or even collapse when geometry deviation occurs during the deposition and is not solved in a timely manner, which will lead to time and cost waste. Moreover, an accurate geometry profile is quite helpful for other quality analysis during the printing process, such as the online stress measurement [9]. Therefore, it is important that the geometry of the printed object is continuously inspected in real time, as more material gets deposited.

Vision cameras and laser line scanners are often employed to assess the geometry of an object being printed via DED [10]. However, though vision cameras can assess the geometry in real-time, only either the track width or track height is measured, but not the whole track profile [11]. On the other hand, laser line scanners are mostly used post-DED, at which point the influence of powder and deposition laser is quite small so that the measuring accuracy is high. Besides, previous studies on geometry assessment have tended to focus on single- or multi-layer straight line deposition; multi-layer deposition of components with sharp features such as intersections or corners,

is important but not well studied. Therefore, the objective of this study is to develop a system capable of conducting real-time 3D geometry assessment during multi-layer deposition of objects with sharp features. There are four main contributions: (1) A geometry assessment system was developed to achieve both real-time inspection and layer-wise inspection during the LP-DED process; (2) In real-time inspection, an image processing method including a novel encoder-decoder based profile completion network was developed to obtain an accurate track profile; and (3) geometry assessment of multi-layer X-shape deposition has been achieved.

This paper is organized as follows. Section 2 gives some background on our research, which includes the working principle of a laser line scanner, a description of LP-DED and geometry assessment during DED. Section 3 explains the developed geometry assessment methodology. Section 4 provides the experimental results and discussion of the proposed methodology. Section 5 concludes the paper by presenting a summary, limitations, and future work.

2. RESEARCH BACKGROUND

2.1 Description of laser line scanner

A laser line scanner is a piece of non-destructive testing (NDT) equipment that has been used successfully to capture the shape of an object. The scanner operates based on the principle of laser triangulation as shown in Figure 2-2. By selecting the bottom of the sensor as a reference as shown on Figure 2-2, the basic triangulation calculation is expressed in equation (1).

$$b_1 = \frac{a_1}{\tan \alpha_1} \quad (1)$$

For laser line scanner, instead of projecting a single point, a laser line is projected on the target surface. After that, the diffusely reflected light of the laser line is detected by a high-quality sensors array called CMOS sensor matrix. Each projected point corresponds to one column on the sensor matrix. Based on the position of the detected laser beam on the corresponding column on sensor matrix, the distance of one measuring point to a defined reference in the sensor (Z coordinate) and can be calculated via triangulation, and the exact position of each point on the laser line (X coordinate) is acquired accordingly.

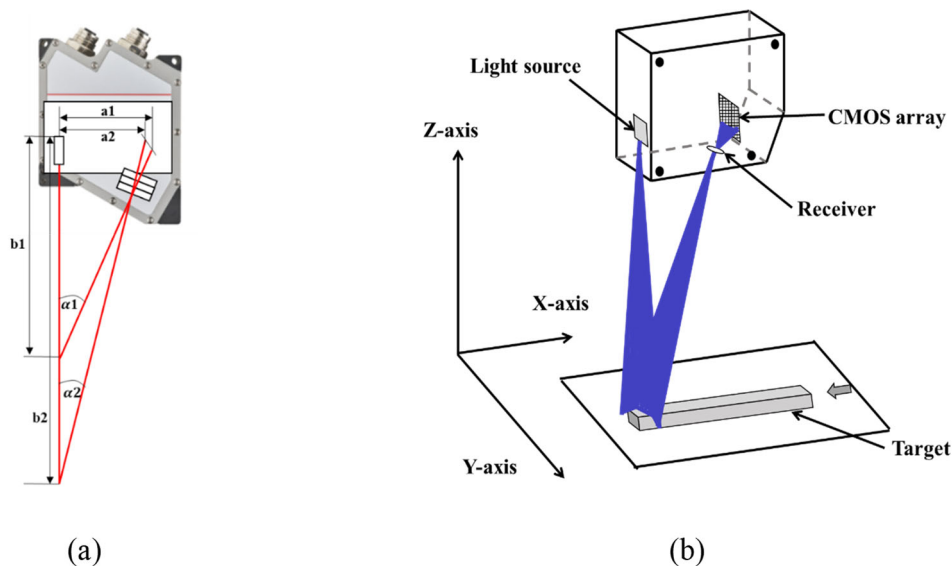


Fig. 1: (a) Principle of optical triangulation, (b) Principle of laser line scanner

In addition, a band filter is embedded right before the CMOS sensor to avoid the reflection of light beyond the expected wavelength, and only captures the reflection of the projected laser line. With respect to laser light, red and blue laser diodes are commonly available for laser line scanners. The red laser scanner is ideal for common measurement tasks especially with extremely dark surfaces whereas the blue laser scanner is ideal for transparent,

organic, and red-hot glowing surfaces. In the DED process, when the high power-density laser is focused on a continuous stream of metal powder, the substrate becomes red-hot glowing surface. Thus, for this study a blue laser diode line scanner is used to achieve an accurate result. In addition, the blue laser is preferred to the red one since it is an extremely sharp-focused laser line that does not penetrate the surface.

2.2 Geometry assessment during DED

The geometry assessment targets include the geometry of the melt pool area and the just solidified area as well as the layer geometry of the deposited object. Much research in recent years has focused on inspecting the geometry of the melt pool, since it can be used for real-time geometry control [10]. Camera-based methods are popularly used to inspect the melt pool geometry, including vision camera and infrared camera. Vision cameras can be used to measure either the width or the height of the melt pool depending on the installation location and the target measurement field [11], while infrared cameras are normally used to measure the width and length of the melt pool [17]. Some recent papers have attempted to estimate the melt pool height using infrared cameras with the help of deep learning methods. However, these methods cannot measure the spatial profile of the melt pool area. The inspection of just solidified area is important as it is reported that this can be used for online stress estimation [9]. Moreover, compared with the melt pool area, the just solidified area might better represent the final geometry of the deposited track since thermal shrinking occurs during the solidification process [18]. The just solidified area is quite close to the melt pool area so that some studies use it for real-time geometry control though there is bound to be a small lag. Similarly, camera-based methods are used but a spatial profile cannot be obtained [19]. While laser line scanners can be used to obtain a special profile [20], its performance are affected by powder reflection and high intensity melting laser during LP-DED process, which prevents it from obtaining accurate spatial profile, thus it is often used for layer-wise geometry inspection rather than real-time geometry inspection. The inspection of layer geometry after printing each layer has been studied as well. This method needs to consider inspection path during the design process, which increases design effort and printing time. However, it is applicable to all kinds of printing shapes and toolpaths. In addition, for layer-wise control which does not need instant feedback, it is a better choice [21]. To address geometry assessment of all three targets, a geometry assessment system is developed in this study which aims to achieve both real-time inspection and layer-wise inspection of the track profile using laser line scanner.

Note that the term “real-time” might be ambiguous, as it has been used in a different sense in the literature from field to field. In this study, inspections with the laser line of a line scanner located at just a solidified area or melting pool area are called real-time inspection, where a small delay relative to the deposition is expected. On the other hand, inspection that takes place after each layer has been printed is called layer-wise inspection, since normally a large delay exists.

3. METHODOLOGY

3.1 Overview of the geometry assessment methodology

For real-time inspection, images are captured during deposition. Here there are three apparent problems that would prevent us from obtaining an accurate profile: (1) powder reflection, (2) melt-influenced area and (3) track profile missing, as illustrated in Fig. 4. The following steps are proposed to overcome these three problems.

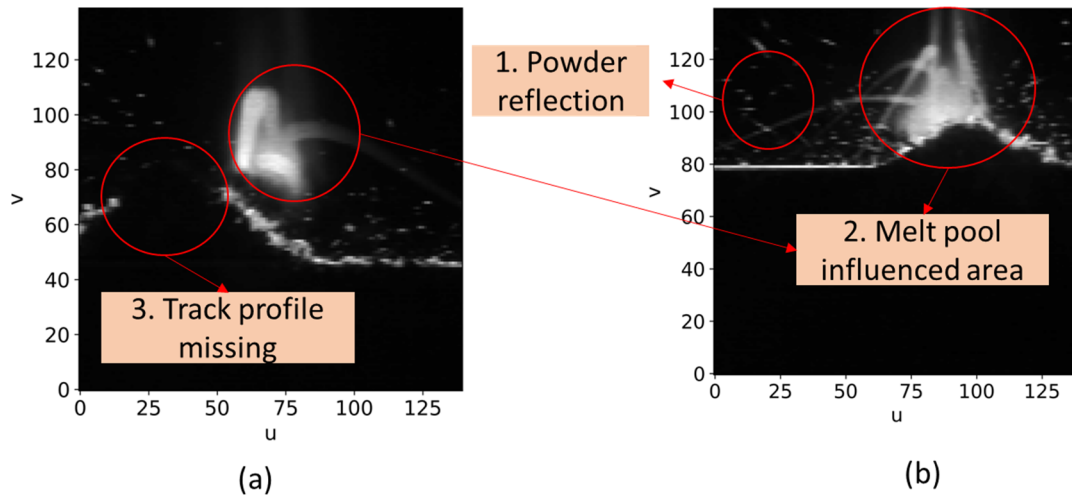


Fig. 4 Problems with raw images: (a) typical profile from real-time inspection of melt pool area, (b) typical profile from real-time inspection of just solidified area

3.2 Powder reflection removal

Firstly, an image enhancement technique, namely contrast stretching, is applied to improve the contrast in each image by converting the original intensity value of a smaller range to a larger range of intensity values, as shown in Eq. (3) and Fig. 5.

$$s = T(r) \tag{3}$$

where r is the input intensity, s is the output intensity, and T is the intensity transformation function. By applying this function, the brighter pixels become even brighter, and darker pixels become even dimmer. Since powder reflection always has lower intensity, it can remove the pixels of powder reflection.

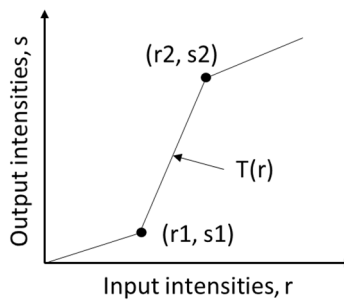


Fig. 5 Powder reflection removal: contrast stretching

3.3 Melt-influenced area removal

To remove the melt-influenced area, a DBSCAN clustering algorithm is applied on the image. As shown in Fig. 6(a), for all non-zero pixels in the image, a core pixel is selected if the pixel has n number of neighbors, where the neighbors are pixels within a distance ϵ from the core pixel. The distance between two pixels is calculated

using Eq. (4):

$$d_{ij} = \sqrt{(u_j - u_i)^2 + (v_j - v_i)^2} \quad (4)$$

where (u_i, v_i) and (u_j, v_j) are the U-V coordinates of pixels i and j . A cluster is formed by recursively taking a core pixel, finding among all of its neighbor pixels that are core pixels, in turn finding all of their neighbors that are core pixels, and so on. After clustering, the cluster with the largest mean v value will be removed. For some images, the melt-influenced area will be connected to the track profile, and the track profile will be removed as shown in Fig. 6 (b). To solve this problem, a modified DBSCAN is proposed by adding an additional coordinate m to represent the distance to the lowest non-zero pixels for each column as illustrated in Fig. 6 (c) and the distance between two pixels is calculated using Eq. (5). After that, the DBSCAN algorithm is applied, and the result can be seen in Fig. 6(d)

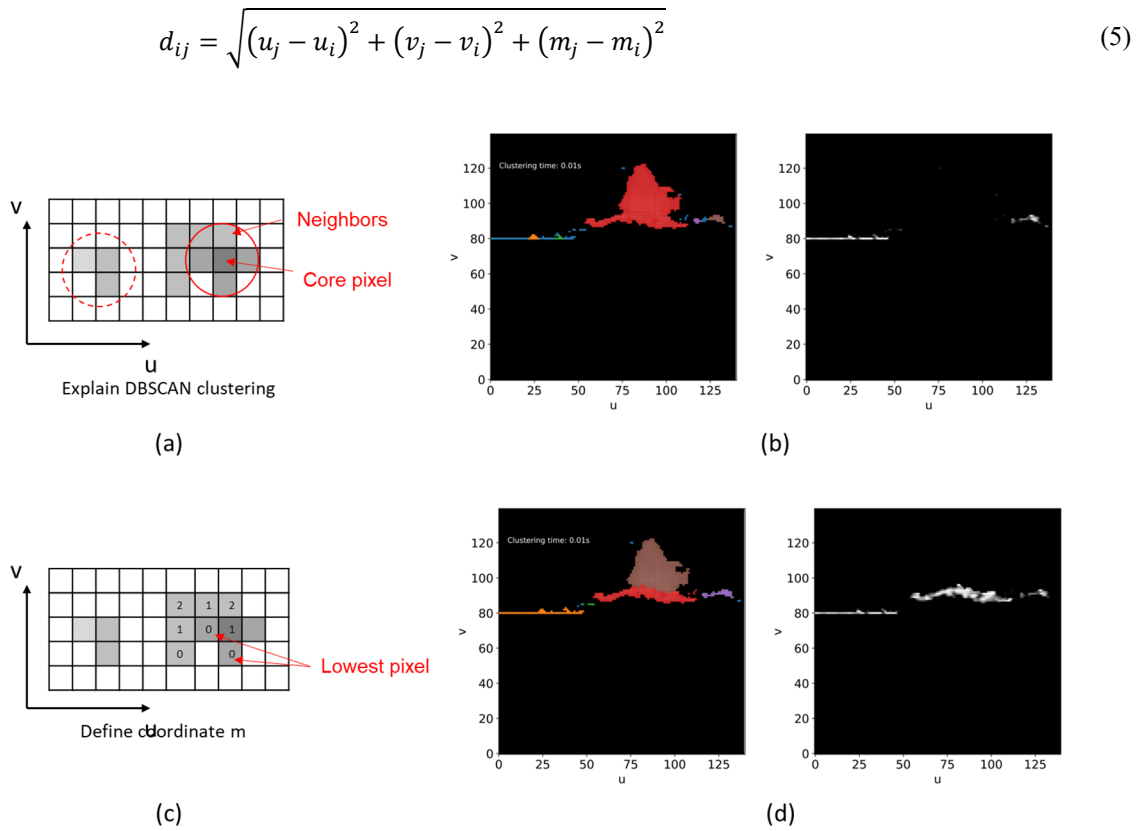


Fig. 6 Melt-influenced area removal: (a) explain DBSCAN clustering on the image, (b) directly apply DSCAN, (c) add coordinate m and (d) apply modified DBSCAN

3.4 Encoder-decoder based profile completion

After melt-influenced area removal, the track profile is extracted. However, there exists severe profile missing problems, which will severely deteriorate the quality of 3D point cloud for geometry assessment. The profile missing problem is mainly due to bad reflection on the deposited metal surfaces, especially when there is high-intensity laser radiation from the printer. As shown in Fig. 7, the cross-sections at different locations on the X-shape represents different types of profile missing, and a pattern can be observed for each track: (1) at the beginning of each track (location A), the opposite side of the melt-pool influenced area are missing for the one-peak cross section; (2) when approaching the intersection (location B), the line scanner captures two-peak cross section and the middle part of the two-peak cross section is missing; (3) at the intersection (location C), the top part of the one-peak cross section is missing; (4) when getting away from the intersection (location D), two

side parts of the two-peak cross section are missing; (5) at the end of each track (location E), same as in location A, the opposite side missing of one-peak cross-section can be observed. For such varied types of profile missing problems, traditional completion methods such as curve fitting [22] or interpolation methods cannot achieve satisfied result, especially for the middle part missing of two-peak cross section.

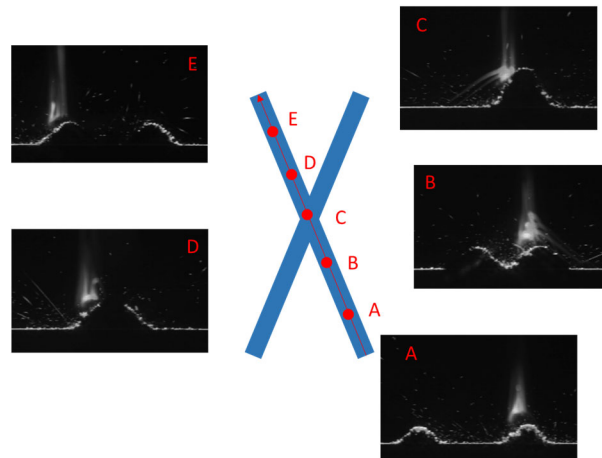


Fig. 7 Track profile missing problem

To complete the track profile in captured images, an encoder-decoder based profile completion algorithm is proposed. The idea of adopting an encoder-decoder based network comes from point cloud completion techniques. Encoder-decoder based networks are widely used in 3D point cloud completion tasks [23], [24], as the encoder can summarize the geometric information from an incomplete input point cloud to form a feature vector, and, based on the feature vector, the decoder will predict the complete shape of the point cloud. The proposed algorithm is revised from DeepLabv3+ [25], which is a popular encoder-decoder network with images as input.

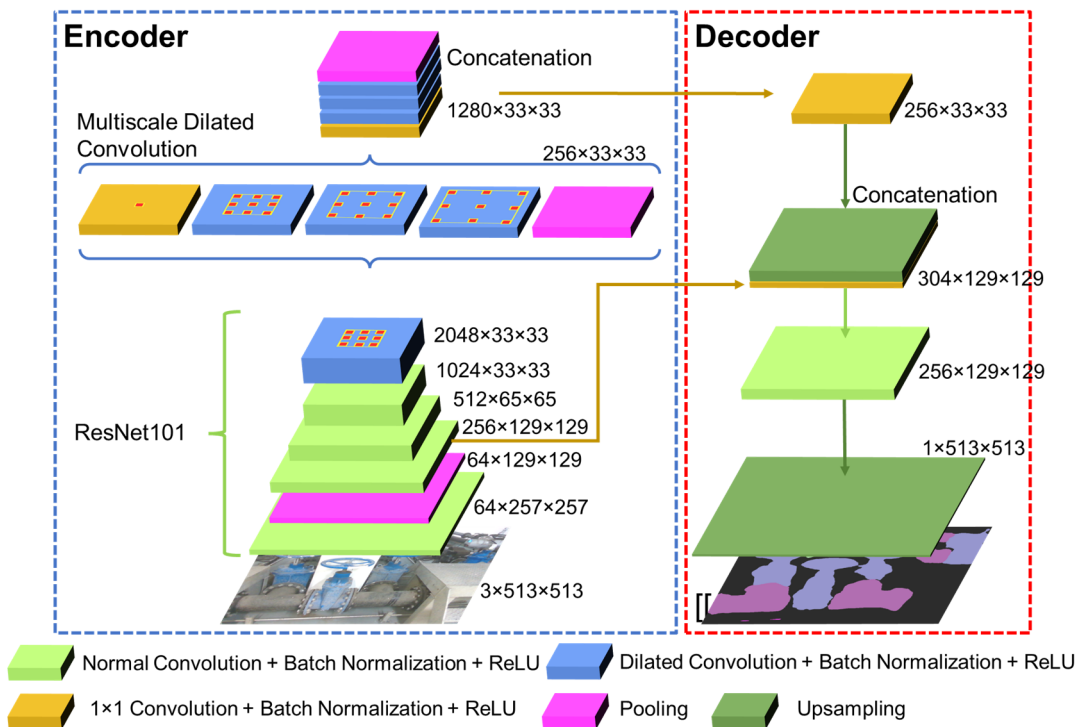


Fig. 8 Proposed encoder-decoder based profile completion network

In this study, the useful information in preprocessed images is the track profile pixels, which take up a small proportion of the whole image. Therefore, to make an efficient use of information in the images, the images from previous steps are further converted to 1D array and fed as input. A novel deeplab1D network is proposed which changes 2D operation in all layers of the DeepLabv3+ network to a 1D operation. Moreover, since previous profiles might provide useful information for the completion of current profile, therefore the previous $(t - 1)$ profiles are considered as input for the proposed network. When t equals 1, only the current profile is considered.

The architecture of the proposed encoder-decoder based network is shown in Fig. 8. First, the image of 140×220 pixels from previous steps is converted into a 1×220 array. For each column of the array of the image, the gravity of the intensity plot on the v axis is taken as one of the values in the 1×220 array. The 1×220 array is inputted into the proposed network, which includes an encoder and a decoder. The encoder consists of a ResNet1D and an ASPP1D module. The ResNet1D module is based on ResNet-101 [26]. The ASPP1D module has evolved from Atrous Spatial Pyramid Pooling (ASPP) [27], which conducts several parallel Atrous convolutions with different rates. An Atrous convolution is described in Eq. (6).

$$y[i] = \sum_k x[i + r \cdot k] w[k] \quad (6)$$

where i is the location on the output feature map y , w is a convolution filter applied over the input feature map x . The Atrous rate r determines the stride that samples the input signal. Note that an Atrous convolution with $r = 1$ is equal to a standard convolution. In the encoder module, the concatenated output from ASPP1D is processed by a 1×1 convolution and an interpolation by a factor of 4, then concatenated with the convolved low-level feature from the ResNet1D. After this concatenation, a few convolutions are applied to refine the features followed by interpolation by a factor of 4 to recover the final output shape (a 1×220 array).

3.5 Point cloud generation

The captured data from real-time inspection and layer-wise inspection is in its local coordinate system. For subsequent geometry assessment, such as comparing as-designed geometry with as-built geometry, the captured data needs to be converted to the global coordinate system. For real-time inspection, the U-V to X-Z coordinates conversion and X-Z coordinate transformation are needed to obtain the point cloud of target cross-section from captured images. While for layer-wise inspection, 2D points are collected, thus only X-Z coordinate transformation is conducted.

Since the commercial line scanner normally uses a CCD sensor to capture its emitted laser reflection on the target surface, this process can be modeled using a pin-hole model, which is the basis camera model based on the perspective projection principle [28].

First, intrinsic calibration is conducted, which is to reconstruct the X-Z coordinates in the real-world coordinate system, given the U-V coordinates in the image coordinate system using the following equation.

$$\begin{bmatrix} x_l \\ z_l \\ 1 \end{bmatrix} = \begin{bmatrix} k_{11}' & k_{12}' & k_{13}' \\ k_{21}' & k_{22}' & k_{23}' \\ k_{31}' & k_{32}' & k_{33}' \end{bmatrix} \begin{bmatrix} u \\ v \\ 1 \end{bmatrix} \quad (10)$$

By getting several pairs of U-V and X-Z coordinates, a least-square solution can be used, and the intrinsic transformation matrix K can be obtained.

Second, after obtaining the X-Z coordinates in the line scanner's local coordinate system (X_L, Z_L) , a translation matrix is needed to convert the X-Z coordinates into the global coordinate system (X_G, Z_G) , which is the extrinsic calibration process. After installing the laser line scanner, a rectangular calibration bar with known dimension is put at the origin of the global coordinate system, thus the as-designed cross section profile of the calibration bar in the global coordinate system can be obtained. Finally, after obtaining coordinates of measure profile in nozzle's coordinate system, the 3D coordinates of the measured profile in the global coordinate system can be calculated by fusing the nozzle's position using Eq. (16).

$$\begin{bmatrix} x_g \\ y_g \\ z_g \end{bmatrix} = \begin{bmatrix} 1 & 0 & 0 & tx_2 \\ 0 & 1 & 0 & ty_2 \\ 0 & 0 & 1 & tz_2 \end{bmatrix} \begin{bmatrix} x_n \\ y_n \\ z_n \\ 1 \end{bmatrix} \quad (16)$$

where the tx_2 , ty_2 and tz_2 are the coordinates of the printing position in the global coordinate system, i.e., the nozzle's position. To obtain the nozzle's position for each captured profile, a log file is extracted from the DED printer during deposition which contains the location of the nozzle and a timestamp at each location.

4. EXPERIMENT AND DISCUSSION

4.1 Experiment setup

The LP-DED printer used in this study is an InssTek MX-400, which is a commercial metal printer equipped with a 5-degree-of-freedom mechanical moving stage, a Ytterbium fiber laser with a wavelength of 1070 nm, a maximum power of 1kW, and a focal laser beam diameter of 800 μm , as well as a metal powder delivery system with shield gas and carrier gas (Argon gas). A 316 L stainless-steel powder with an average particle size of 100 μm was used for deposition and a substrate using the same material as the powder with dimensions 100 mm \times 50 mm \times 10 mm was placed on the moving stage.

Two laser line scanners (Micro-Epsilon scanCONTROL 3000-25/BL), an inclined line scanner and an upright line scanner (Fig. 13), are installed for real-time and layer-wise inspection, respectively. Calibrations are conducted for both line scanners to get the transformation matrix used for 3D point cloud generation before deposition. For the inclined line scanner, intrinsic and extrinsic calibration are conducted; for the upright line scanner, only extrinsic calibration is needed. The exposure time was set to 20 ms (determined based on experience) to get a better reflection from the metal surfaces. The deposited object is a 20-layer X-shaped object. Two experiments are conducted: Experiment 1: deposition with real-time inspection of melt pool area ($d = 0\text{mm}$) and layer-wise inspection; Experiment 2: deposition with real-time inspection of just solidified area ($d = 3\text{mm}$) and layer-wise inspection.

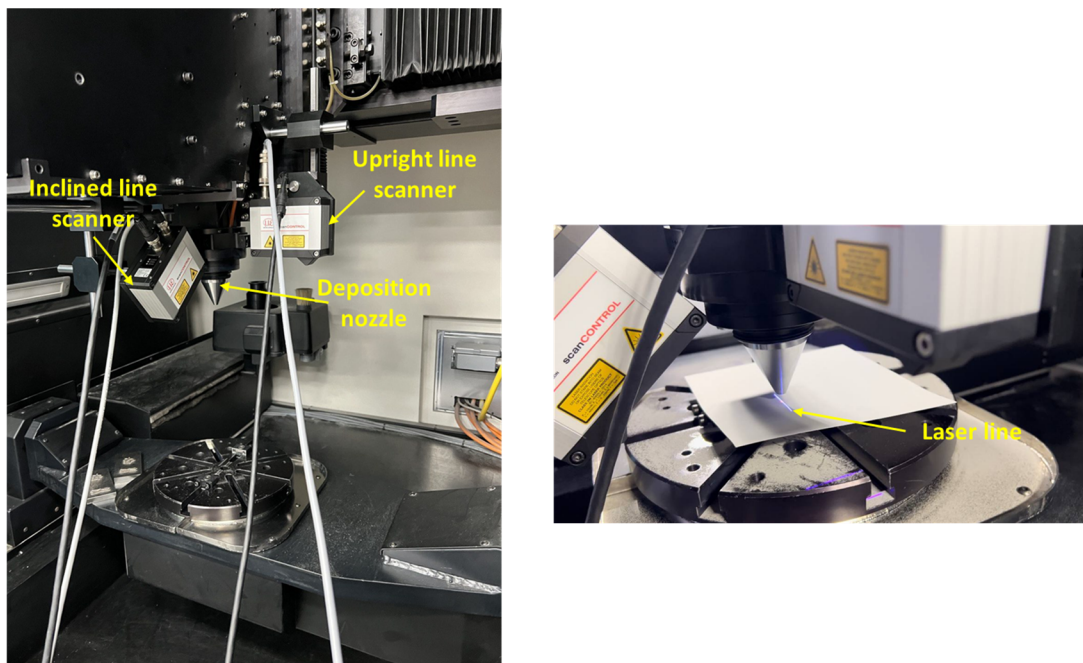


Fig. 13 Experiment setup: Geometry assessment system

4.2 Processing result

During the deposition of each layer, the inclined line scanner with laser line pointing at the melt pool or just solidified area captures and transfers images to the software for processing. After the deposition of each layer, layer-wise inspection is conducted by the upright line scanner, and point profiles are collected. For layer-wise inspection, 2D points of each cross-section are obtained and 3D point cloud data can be generated using extrinsic calibration matrix and fusing printer information. For real-time inspection, powder reflection removal and melt-influenced area removal are conducted for each image. Then the developed encoder-decoder based profile completion network is used to complete the profile on each image and the U-V coordinates are obtained. Finally, a 3D point cloud data of the deposition X-shape object in the global coordinate system can be generated using the proposed method.

Two experiments are conducted and each with 20 layers of data collected. Experiment 1 collects 1167 images and Experiment 2 collects 1157 images in total. Given the traverse speed of the printer (10 mm/s) and the total tool path length of each deposition (993.86 mm), the actual profile rate of the real-time inspection is about 12 frames per second. In this study, the paired image data from experiment 1 is used for model training and validation, which is divided into training and validation data in a ratio of 0.8, 0.2, respectively. The collected data from experiment 2 is used for model testing. The training process was conducted on GPU (NVIDIA GeForce GTX1080) using Python 3.9, Pytorch 11.7 and CUDA 11.8. Since previous profile is considered, t equals 1 to 5 are considered. For each t value, 80 epochs are trained, the validation dataset is used to choose the best model, then the best model is used for testing.

Root mean squared error (RMSE) was calculated between the output prediction array and the ground truth array. The average RMSE of all profiles in each layer was obtained for each t for comparison (Table 4). For higher layers, the RMSE becomes larger. This is due to the fact that when the layer height becomes higher, the sides of the deposited object will have a more inclined angle of 90 degrees, resulting in a worse reflection of the laser from the line scanner projected on the side of the deposited object. Thus, there will be a more serious profile missing problem for the higher layers, making it more difficult to complete the profile. In addition, when the absolute deposition height increases, the network prediction error also tends to increase, but the proportion of the error with respect to absolute deposition height may remain the same. Therefore, an RMSE-H ratio is calculated for each layer, which is the RMSE error divided by the design height (Table 4). As seen, there is not much difference in the RMSE-H ratio for each layer. The RMSE-H ratio of the first few layers is larger. Considering that the profiles of the first five layers are not seriously missing and the completion model may not be effective in such cases, the profile completion can be applied to the higher layers without the first five layers. When more previous layers are involved, there is little difference in the performance of the proposed model. A slight decrease of RMSE can be observed when t equals 2. Therefore, the model with $t = 2$ is finally selected as the profile completion model in our geometry assessment system, which can generate point cloud with an RMSE of 0.21 mm compared with the ground truth.

Table 4: Test results of the proposed model for different values of t

Test result		As-designed height (mm)	RMSE (mm)					RMSE-H ratio				
			$t = 1$	$t = 2$	$t = 3$	$t = 4$	$t = 5$	$t = 1$	$t = 2$	$t = 3$	$t = 4$	$t = 5$
Layer	1	0.2	0.03	0.03	0.03	0.04	0.03	16%	14%	16%	18%	15%
	2	0.4	0.06	0.05	0.06	0.06	0.06	14%	13%	14%	14%	14%
	3	0.6	0.07	0.07	0.08	0.08	0.08	12%	11%	13%	13%	14%
	4	0.8	0.10	0.09	0.10	0.10	0.11	12%	11%	13%	12%	14%
	5	1	0.11	0.10	0.11	0.12	0.13	11%	10%	11%	12%	13%
	6	1.2	0.13	0.12	0.14	0.14	0.16	11%	10%	12%	11%	13%

7	1.4	0.16	0.15	0.18	0.18	0.19	12%	11%	13%	13%	13%
8	1.6	0.16	0.17	0.18	0.19	0.20	10%	10%	11%	12%	13%
9	1.8	0.20	0.18	0.20	0.19	0.21	11%	10%	11%	11%	12%
10	2	0.19	0.18	0.20	0.19	0.21	9%	9%	10%	10%	11%
11	2.2	0.22	0.20	0.22	0.22	0.23	10%	9%	10%	10%	11%
12	2.4	0.23	0.23	0.23	0.22	0.25	10%	10%	10%	9%	10%
13	2.6	0.25	0.24	0.25	0.23	0.26	9%	9%	9%	9%	10%
14	2.8	0.28	0.29	0.28	0.30	0.31	10%	10%	10%	11%	11%
15	3	0.27	0.27	0.28	0.30	0.33	9%	9%	9%	10%	11%
16	3.2	0.31	0.29	0.30	0.31	0.33	10%	9%	9%	10%	10%
17	3.4	0.38	0.36	0.36	0.38	0.37	11%	10%	11%	11%	11%
18	3.6	0.40	0.38	0.39	0.39	0.39	11%	11%	11%	11%	11%
19	3.8	0.40	0.38	0.38	0.41	0.41	11%	10%	10%	11%	11%
20	4	0.43	0.42	0.42	0.44	0.45	11%	11%	10%	11%	11%
Overall		0.22	0.21	0.22	0.22	0.24					

5. CONCLUSION

This study has developed a real-time geometry assessment methodology for LP-DED using laser line scanner. A geometry assessment system has also been developed to achieve real-time inspection of the melt pool area and the just solidified area, as well as layer-wise inspection of the layers' geometry. An image processing method has been proposed including powder reflection removal, melt-influenced area removal and an encoder-decoder based profile completion network to obtain track profile on images. Then a point cloud generation method was developed including U-V to X-Z coordinates conversion, X-Z coordinate transformation, and 3D point cloud generation by fusing printer information. Experiments have been conducted to validate the proposed method and the result shows that an average RMSE of 0.21 mm can be achieved from point cloud comparison between the point clouds obtained in realtime and obtained layer-wise. The proposed real-time inspection method was able to achieve better performance compared with the line scanner's built-in method, and the developed encoder-decoder profile completion model has been validated which outperforms baseline model. The deposition heights of the melt pool and solidified layer were compared, and the result showed that the differences were not significant using the proposed method.

ACKNOWLEDGEMENT

This work was supported by the National Research Foundation of Korea (NRF) grant funded by the Korean government (MSIT) (grant number: 2019R1A3B3067987).

REFERENCES

- [1] J. Xiong, G. Zhang, Adaptive control of deposited height in GMAW-based layer additive manufacturing, *Journal of Materials Processing Technology*. 214 (2014) 962–968. <https://doi.org/10.1016/j.jmatprotec.2013.11.014>.
- [2] L. Tang, R.G. Landers, Melt Pool Temperature Control for Laser Metal Deposition Processes—Part II: Layer-to-Layer Temperature Control, *Journal of Manufacturing Science and Engineering*. 132 (2010) 011011. <https://doi.org/10.1115/1.4000883>.
- [3] S.K. Everton, M. Hirsch, P. Stravroulakis, R.K. Leach, A.T. Clare, Review of in-situ process monitoring and in-situ metrology for metal additive manufacturing, *Materials & Design*. 95 (2016) 431–445. <https://doi.org/10.1016/j.matdes.2016.01.099>.
- [4] H.-W. Hsu, Y.-L. Lo, M.-H. Lee, Vision-based inspection system for cladding height measurement in Direct Energy Deposition (DED), *Additive Manufacturing*. 27 (2019) 372–378. <https://doi.org/10.1016/j.addma.2019.03.017>.
- [5] N. Decker, Y. Wang, Q. Huang, Efficiently registering scan point clouds of 3D printed parts for shape accuracy assessment and modeling, *Journal of Manufacturing Systems*. 56 (2020) 587–597. <https://doi.org/10.1016/j.jmsy.2020.04.001>.
- [6] C. Xia, Z. Pan, J. Polden, H. Li, Y. Xu, S. Chen, Y. Zhang, A review on wire arc additive manufacturing: Monitoring, control and a framework of automated system, *Journal of Manufacturing Systems*. 57 (2020) 31–45. <https://doi.org/10.1016/j.jmsy.2020.08.008>.
- [7] Micro-Epsilon Messtechnik, Laser line triangulation | Micro-Epsilon, Micro-Epsilon Messtechnik. (n.d.). <https://www.micro-epsilon.com> (accessed December 20, 2022).
- [8] L. Yang, K. Hsu, B. Baughman, D. Godfrey, F. Medina, M. Menon, S. Wiener, *Additive Manufacturing of Metals: The Technology, Materials, Design and Production*, Springer International Publishing, Cham, 2017. <https://doi.org/10.1007/978-3-319-55128-9>.
- [9] I. Jeon, L. Yang, K. Ryu, H. Sohn, Online melt pool depth estimation during directed energy deposition using coaxial infrared camera, laser line scanner, and artificial neural network, *Additive Manufacturing*. 47 (2021) 102295. <https://doi.org/10.1016/j.addma.2021.102295>.
- [10] D. Tyralla, H. Köhler, T. Seefeld, C. Thomy, R. Narita, A multi-parameter control of track geometry and melt pool size for laser metal deposition, *Procedia CIRP*. 94 (2020) 430–435. <https://doi.org/10.1016/j.procir.2020.09.159>.
- [11] B.T. Gibson, Y.K. Bandari, B.S. Richardson, W.C. Henry, E.J. Vetland, T.W. Sundermann, L.J. Love, Melt pool size control through multiple closed-loop modalities in laser-wire directed energy deposition of Ti-6Al-4V, *Additive Manufacturing*. 32 (2020) 100993. <https://doi.org/10.1016/j.addma.2019.100993>.
- [12] Y. Lu, G. Sun, X. Xiao, J. Mazumder, Online Stress Measurement During Laser-aided Metallic Additive Manufacturing, *Sci Rep*. 9 (2019) 7630. <https://doi.org/10.1038/s41598-019-39849-0>.
- [13] S. Kim, I. Jeon, H. Sohn, Infrared thermographic imaging based real-time layer height estimation during directed energy deposition, *Optics and Lasers in Engineering*. 168 (2023) 107661. <https://doi.org/10.1016/j.optlaseng.2023.107661>.
- [14] R. Sampson, R. Lancaster, M. Sutcliffe, D. Carswell, C. Hauser, J. Barras, The influence of key process parameters on melt pool geometry in direct energy deposition additive manufacturing systems, *Optics & Laser Technology*. 134 (2021) 106609. <https://doi.org/10.1016/j.optlastec.2020.106609>.
- [15] M. Borish, B.K. Post, A. Roschli, P.C. Chesser, L.J. Love, K.T. Gaul, Defect Identification and Mitigation Via Visual Inspection in Large-Scale Additive Manufacturing, *JOM*. 71 (2019) 893–899. <https://doi.org/10.1007/s11837-018-3220-6>.
- [16] M. Faes, F. Vogeler, K. Coppens, H. Valkenaers, W. Abbeloos, T. Goedeme, E. Ferraris, Process Monitoring of Extrusion Based 3D Printing via Laser Scanning, (2014). <https://doi.org/10.13140/2.1.5175.0081>.

- [17] W. Lin, H. Shen, J. Fu, S. Wu, Online quality monitoring in material extrusion additive manufacturing processes based on laser scanning technology, *Precision Engineering*. 60 (2019) 76–84. <https://doi.org/10.1016/j.precisioneng.2019.06.004>.
- [18] A. Vandone, S. Baraldo, A. Valente, Multisensor Data Fusion for Additive Manufacturing Process Control, *IEEE Robot. Autom. Lett.* 3 (2018) 3279–3284. <https://doi.org/10.1109/LRA.2018.2851792>.
- [19] A. Heralić, A.-K. Christiansson, B. Lennartson, Height control of laser metal-wire deposition based on iterative learning control and 3D scanning, *Optics and Lasers in Engineering*. 50 (2012) 1230–1241. <https://doi.org/10.1016/j.optlaseng.2012.03.016>.
- [20] R.C. Gonzalez, R.E. Woods, *Digital image processing*, Pearson, New York, NY, 2018.
- [21] D. Deng, DBSCAN Clustering Algorithm Based on Density, in: 2020 7th International Forum on Electrical Engineering and Automation (IFEEA), 2020: pp. 949–953. <https://doi.org/10.1109/IFEEA51475.2020.00199>.
- [22] P.G. Guest, P.G. Guest, *Numerical Methods of Curve Fitting*, Cambridge University Press, 2012.
- [23] L.-C. Chen, Y. Zhu, G. Papandreou, F. Schroff, H. Adam, Encoder-Decoder with Atrous Separable Convolution for Semantic Image Segmentation, (2018). <http://arxiv.org/abs/1802.02611> (accessed October 28, 2022).
- [24] W. Yuan, T. Khot, D. Held, C. Mertz, M. Hebert, PCN: Point Completion Network, in: 2018 International Conference on 3D Vision (3DV), IEEE, Verona, 2018: pp. 728–737. <https://doi.org/10.1109/3DV.2018.00088>.
- [25] X. Yu, Y. Rao, Z. Wang, Z. Liu, J. Lu, J. Zhou, PoinTr: Diverse Point Cloud Completion with Geometry-Aware Transformers, in: 2021 IEEE/CVF International Conference on Computer Vision (ICCV), IEEE, Montreal, QC, Canada, 2021: pp. 12478–12487. <https://doi.org/10.1109/ICCV48922.2021.01227>.
- [26] K. He, X. Zhang, S. Ren, J. Sun, Deep Residual Learning for Image Recognition, in: 2016: pp. 770–778. https://openaccess.thecvf.com/content_cvpr_2016/html/He_Deep_Residual_Learning_CVPR_2016_paper.html (accessed December 5, 2022).
- [27] L.-C. Chen, G. Papandreou, F. Schroff, H. Adam, Rethinking Atrous Convolution for Semantic Image Segmentation, (2017). <https://doi.org/10.48550/arXiv.1706.05587>.
- [28] J. Santolaria, J.J. Pastor, F.J. Brozed, J.J. Aguilar, A one-step intrinsic and extrinsic calibration method for laser line scanner operation in coordinate measuring machines, *Meas. Sci. Technol.* 20 (2009) 045107. <https://doi.org/10.1088/0957-0233/20/4/045107>.